Interaction of NO with Nanosized Ru-, Pd-, and Pt-Doped SnO_2: Electron Paramagnetic Resonance, Mössbauer, and Electrical Investigation

Carmen Canevali,[†] Claudio Maria Mari,[†] Mariachiara Mattoni,[†] Franca Morazzoni,*[,†] Luca Nodari,[‡] Riccardo Ruffo,[†] Umberto Russo,[‡] and Roberto Scotti[†]

Dipartimento di Scienza dei Materiali, INSTM-UdR Milano-Bicocca, Università di Milano-Bicocca, Via Cozzi 53, 20125 Milano, Italy, and Dipartimento di Scienze Chimiche, Via Marzolo 1, 35131 Padova, Italy

Received: November 30, 2004; In Final Form: February 2, 2005

The mechanism of NO interaction with nanosized Ru(Pd,Pt)-doped SnO_2 was studied by electron paramagnetic resonance, Mössbauer, and electric resistance measurements. Three steps were proposed for the reaction between the semiconductor oxide and the gaseous component: (i) the formation of bielectronic oxygen vacancies (V_o) in SnO_2; (ii) their single-ionization ($V_o^\bullet$) with injection of electrons into the SnO_2 conduction band; (iii) the subsequent transfer of electrons from $V_o^\bullet$ to $[Ru(Pd,Pt)]^{4+}$. The last process induces the formation of further oxygen vacancies which reduce the transition metal centers to lower oxidation states; the redox processes is enhanced and the electrical resistance in transition metal-doped SnO_2 is stronger modified with respect to the undoped material.

Introduction

It is well-known the electrical sensitivity of SnO_2, a base material for semiconductor gas sensors, is enhanced by its doping with transition metals. Two main models were proposed to explain this effect: the first based on the chemical interaction of gases with the metal (e.g. dissociative chemisorption of H_2 on noble metal centers) and the second on the redox processes between interacting gases and metal centers.[1] Nevertheless the role of the doping metal in the gas-oxide reaction mechanism is still under discussion.

To improve the knowledge of the electron-transfer processes between the reducing gas and the metal centers, we studied in previous papers the interaction of CO with SnO_2-based materials, either as a nanopowder or as a nanosized thin film. It was suggested that the redox processes involve Pt- and Ru-doping centers[2−5] through an undirect mechanism mediated by the oxygen defects. The main steps are the formation and ionization of oxygen vacancies

$$O_o + CO \leftrightarrow CO_2 + V_o \quad (1)$$

$$V_o \leftrightarrow V_o^\bullet + e^- \quad (2)$$

(O_o is the oxide anion in its regular oxygen site, V_o the neutral oxygen vacancy, and $V_o^\bullet$ the singly ionized oxygen vacancy) followed by the transfer of electrons from $V_o^\bullet$ into the transition metal centers, according to

$$Pt(Ru)^{4+} + nV_o^\bullet \leftrightarrow Pt(Ru)^{(4-n)+} + nV_o^{\bullet\bullet} \quad (3)$$

($V_o^{\bullet\bullet}$ is the doubly ionized oxygen vacancy, $n = 1-4$ for Pt, and $n = 1$ for Ru). This electron-transfer reaction shifts the equilibria of reactions 1 and 2 toward the right-hand side increasing the number of V_o defects and of electrons injected into the conduction band, with respect to undoped SnO_2. The reduced transition metal center $Pt(Ru)^{(4-n)+}$ is also responsible for the reduction of oxygen and the successive interaction with Sn_{Sn}:

$$nSn_{Sn} + nO_2 + Pt(Ru)^{(4-n)+} \leftrightarrow Pt(Ru)^{4+} + nSn_{Sn}-O_2^- \quad (4)$$

(Here Sn_{Sn} is a tin atom in the lattice site.) Such conclusions were obtained by different and complementary investigation techniques depending on the type of sample: powder,[2] thin film[3,5] or both.[4]

Recently our interest was addressed to investigate the interaction of SnO_2-based materials with NO. There is in fact large interest to study the surface reactions and the electrical response of semiconductor oxides that had undergone NO contact not only because the mechanism of NO interaction is still far from being fully understood but also for nowadays because of the important environmental issue.

The preliminary study[6] concerned the surface reactivity of undoped nanocrystalline SnO_2; it was demonstrated NO behaves as a reducing agent (either forming oxygen vacancies or injecting electrons into the SnO_2 conduction band) and the NO_2^- and NO_3^- surface chemisorption hinders the NO reducing effects.

Following up the above results, we here investigate the effects of the doping metal (Ru, Pd, and Pt) on the NO interaction with SnO_2. EPR and Mössbauer investigations were performed on Ru(Pd,Pt)-doped SnO_2 nanopowders, while measurements of electrical resistance were performed on thin films of the same materials; both sets of specimens were obtained by the sol−gel route. Furthermore, to compare the effects of different gases, the metal:Sn molar ratios were the same as used in the studies of CO interaction.[2−5] Spectroscopic, spectromagnetic, and electrical responses of samples were obtained by treatment under NO/argon mixture to avoid the oxidation of nitrogen monoxide.

Experimental Section

Reactants. Tetrakis(*tert*-butoxy)tin(IV), $[Sn(OBu^t)_4]$, was prepared according to the literature.[7] Tris(acetylacetonato)-

* Corresponding author. E-mail: franca.morazzoni@mater.unimib.it. Phone: 0039 02 64485123. Fax: 0039 02 64485400.
[†] Università di Milano-Bicocca.
[‡] Dipartimento di Scienze Chimiche.

10.1021/jp040740k CCC: $30.25
Published on Web 03/18/2005

ruthenium(III), [Ru(acac)$_3$], bis(acetylacetonato)palladium(II), [Pd(acac)$_2$], and bis(acetylacetonato)platinum(II), [Pt(acac)$_2$], were Aldrich pure chemicals.

Pure (argon, air) and mixed [NO(495 ppm)/argon] gases were purchased from SAPIO.

Preparation of Ru(Pd,Pt)-Doped SnO_2. *Powders.* The sol phase was prepared by mixing and stirring, at room temperature, 12 mL of a solution of [Sn(OBu^t)$_4$] in absolute anhydrous ethanol (500 mg mL^{-1}) and 30 mL of an ethanol−acetylacetone (4:1 v:v) solution of [Ru(acac)$_3$], [Pd(acac)$_2$], or [Pt(acac)$_2$] (3.75×10^{-6} mol mL^{-1}; metal:Sn molar ratio 0.008). After a few minutes, 10 mL of an ethanol−water solution (4:1 v:v) was added and the sol phase put into the thermostatic chamber at 35 ± 1 °C. The sol−gel transition occurred within about 1−2 days. The homogeneous, without evident phase separation, gel was dried under vacuum (10^{-2} Torr) at room temperature, and the xerogel powder was obtained. The thermal treatment of the powdered [Ru(acac)$_3$]−, [Pd(acac)$_2$]−, [Pt(acac)$_2$]−SnO_2 xerogels, at 673 K for 4 h in an air stream (30 cm^3 min^{-1}), produced the different doped SnO_2. The full elimination of the acetylacetonate ligand was monitored by infrared spectroscopy.[2]

X-ray diffraction analysis of samples confirmed the cassiterite structure. The average particle size was evaluated to be in the range 6−10 nm.

Hereafter these samples will be labeled as $RuSnO_2$673, $PdSnO_2$673, and $PtSnO_2$673, respectively.

Thin Films. Metal precursor solutions were obtained by dissolving [Ru(acac)$_3$] (0.1089 g), [Pd(acac)$_2$] (0.8330 g), or [Pt(acac)$_2$] (0.1064 g) in 15 mL of an ethanol−acetylacetone solution (1:1 v:v).

The sol phase was prepared by mixing under nitrogen atmosphere:

(i) 2.50 mL of a solution of [Sn(OBu^t)$_4$] (360 mg mL^{-1}) in anhydrous ethanol−acetylacetone (3.85:1 v:v; corresponding to 2.19 mmol of Sn);

(ii) 3.00 mL of the metal precursor solution (corresponding to 5.47×10^{-2} mmol of metal; metal:Sn molar ratio 0.008);

(iii) 1.52 mL of ethanol and 0.48 mL of acetylacetone;

(iv) 1.00 mL of an ethanol−water solution (4:1 v:v; corresponding to 11.1 mmol of H_2O).

The solution was transferred into a capillary viscosimeter and kept in the thermostatic chamber at 35 ± 1 °C. After 24 h, 0.10 mL of ethanol−water solution (4:1 v:v; corresponding to 1.11 mmol of H_2O) was further introduced; the addition was repeated every 24 h until the sol-phase viscosity was 2.5 cSt, a value suitable for the spin-coating deposition.

Films were deposited by the spin-coating procedure (spin rate 2000 rpm), dried at room temperature, and then annealed at 673 K in air stream (30 cm^3 min^{-1}) for 2 h. The thermal treatment fully decomposed the acetylacetonate ligand, and no residual organic contaminants were left in the film.[2] SQ1 quartz slides (10 × 20 mm, 0.25 mm thickness) were used as substrates. Two successive depositions were performed on the same substrate, each of them by the procedure above-described; a final thermal treatment in air stream at 673 K for 2 h was carried out. The thickness of films, measured by a Tencor P-10 surface profiler, was about 80 nm for a single deposition and about 160 nm for the double deposition. All the films, checked for the microstructure by glancing incidence X-ray diffraction analysis (GIXRD), showed the cassiterite structure. The average particle size was about 3 nm. Details of the GIXRD investigation were reported in refs 3 and 4. The films were labeled as the corresponding powdered samples.

TABLE 1: Treatments of M−SnO_2 Powders (M = Ru, Pt, Pd)

sample	treatment	gas stream (30 cm^3 min^{-1})	label
xerogel M(acac)$_n$−SnO_2[a]	673 K, 4 h	air	$MSnO_2$673
	Sequence A		
$MSnO_2$673	623 K, 90 min	air	$MA_1$623
$MA_1$623	623 K, 30 min	NO (495 ppm)/Ar	$MA_2$623
$MA_2$623	RT,[b] 10 min	air	$MA_3$623
	Sequence B		
$MSnO_2$673	623 K, 90 min	Ar	$MB_1$623
$MB_1$623	623 K, 30 min	NO (495 ppm)/Ar	$MB_2$623
$MB_2$623	623 K, 60 min	Ar	$MB_3$623

[a] M(acac)$_n$ = Ru(acac)$_3$, Pt(acac)$_2$, Pd(acac)$_2$. [b] RT = room temperature.

Electron Paramagnetic Resonance (EPR) Measurements. EPR spectra were recorded on powdered samples by using a conventional Bruker EMX spectrometer operating at the X-band frequency and magnetic field modulation of 100 kHz, with a microwave power of 10 and 5 mW and a modulation amplitude of 10 and 3 G. The *g* values were calculated by comparison with a diphenylpicrylhydrazyl (DPPH) standard sample (g = 2.0036). The amounts of paramagnetic species were calculated by double integration of the resonance line area, taking as reference the area of the Bruker weak pitch (9.7×10^{12} ± 5% spin cm^{-1}) in the case of $V_o^{\bullet}$ and $Sn_{Sn}-O_2^-$ centers and the area of the [Ru(acac)$_3$]−SnO_2 xerogel sample (with Ru/Sn 0.008 molar ratio) in the case of transition metal centers. The resonance lines were simulated by the Bruker WINEPR SimFonia program.

Powdered samples were put into a quartz apparatus suitable for both gas flow interaction and EPR measurements. After each thermal gas treatment, the samples were quenched at room temperature (in about 5 min) and EPR spectra were recorded at 113 K, under the same atmosphere. In the case of air, the spectra were recorded under argon atmosphere, to avoid line broadening due to the possible interaction between molecular oxygen and paramagnetic surface oxygen species.

Two different sequences, A and B, of gas treatments were adopted. Table 1 summarizes the treatments and the sample label.

Sequence A. (1) Ru(Pd,Pt)$SnO_2$673 samples were treated in dry air stream (30 cm^3 min^{-1}) for 90 min at 623 K (samples $RuA_1$623, $PdA_1$623, and $PtA_1$623).

(2) A NO (495 ppm)/argon mixture was passed over samples Ru(Pd,Pt)$A_1$623 (30 cm^3 min^{-1}) at 623 K, and the contact was maintained for 30 min (samples $RuA_2$623, $PdA_2$623, and $PtA_2$623).

(3) Then the samples Ru(Pd,Pt)$A_2$623 were exposed to dry air stream (30 cm^3 min^{-1}) at room temperature for 10 min (samples $RuA_3$623, $PdA_3$623, and $PtA_3$623).

Sequence B. (1) Ru(Pd, Pt)$SnO_2$673 samples were treated under a flowing argon stream (30 cm^3 min^{-1}) for 90 min at 623 K (samples $RuB_1$623, $PdB_1$623, and $PtB_1$623).

(2) A NO/argon stream (30 cm^3 min^{-1}) was passed over samples Ru(Pd,Pt)$B_1$623 at 623 K, and the contact was maintained for 30 min (samples $RuB_2$623, $PdB_2$623, and $PtB_2$623).

(3) Then the samples Ru(Pd,Pt)$B_2$623 were treated again under a flowing argon stream (30 cm^3 min^{-1}) for 60 min at 623 K (samples $RuB_3$623, $PdB_3$623, and $PtB_3$623).

It has to be pointed out that the EPR investigation was performed at a temperature very different from that of the contact with gases, at the sensor working temperature, under

the hypothesis that the gas−surface equilibria were quenched. Thus, the trend in the amount of paramagnetic species, not their absolute value, may be associated with the redox processes discussed by the electric measurements.

The results of the EPR investigation reported for samples treated at 623 K by sequences A and B did not vary if treatments were performed at 573 K, except for a slightly lower amount of paramagnetic transition metal centers. Lower temperatures were not explored as the electrical responses for Ru- and Pd-doped samples were negligible (see electrical properties).

Mössbauer Measurements. Mössbauer experiments were performed at 80.0 K; the source, $Ca^{119m}SnO_3$, nominal stregth 15 mCi, New England Nuclear Corp., was at room temperature and moved with constant acceleration, giving a triangular waveform. Suitable computer programs were employed in the fitting procedure of the experimental spectra to Lorentzian line shapes by using least-squares minimization techniques. The isomer shift data are relative to room-temperature $CaSnO_3$. Samples were prepared by finely grinding about 50.0 mg of powder and mixing with vaseline. The suspension was inserted into a lead container and placed inside the cryostat. All the manipulations were carried out in a glovebox under nitrogen atmosphere. The results are reported in Table 2.

As in the case of paramagnetic centers, the differences in Sn electronic properties observed by Mössbauer spectroscopy have to be considered as a behavior trend, because the spectra were taken at a temperature very different from those really modifying the SnO_2 electric properties.

Electrical Measurements. Electrical investigation was performed on double layered films deposited on SQ1 quartz slides (10 mm × 20 mm, 0.25 mm thickness). Two gold films (10 mm × 4 mm) were deposited at a distance of about 2 mm from each other on the thin films by the dc sputtering technique. Such a procedure was carried out on films after the last annealing in an air stream at 673 K. The samples were put in a quartz chamber and placed in an oven, and the measurements were performed at 473, 523, 573, and 623 K for Pt-doped samples and at 523, 573, and 623 K for Ru- and Pd-doped samples. At lower temperatures the electrical response resulted as too low to be measured. The electrical resistance was measured by a Keithley 617 programmable electrometer. The data acquisition was controlled by the PC connected to the electrometer. Two sequences of gas treatments, A and B, were adopted.

Sequence A. The sensing element was equilibrated in air flow (30 $cm^3\ min^{-1}$) at the selected temperature, and then a NO (495 ppm)/Ar mixture was introduced (30 $cm^3\ min^{-1}$) up to equilibrium conditions. The starting resistance conditions of the film were restored by air equilibration, before introducing again the NO/Ar mixture. S_A is the electrical response defined as ratio between the film resistance under flowing air and under flowing NO/Ar mixture, respectively.

Sequence B. Alternatively, the sensing element was equilibrated in argon flow (30 $cm^3\ min^{-1}$) at the selected temperature and then a NO (495 ppm)/Ar mixture was introduced (30 $cm^3\ min^{-1}$) up to equilibrium conditions. The starting conditions of the film were restored by argon equilibration, before introducing again the NO/Ar mixture. S_B is the electrical response defined as ratio between the film resistance under flowing argon and under flowing NO/Ar mixture, respectively.

Results and Discussion

EPR Investigation. *Sequence A.* Ru−SnO_2. EPR spectra of both $RuSnO_2673$ and RuA_1623 samples (Figure 1, line a) showed the disappearing, under the oxidative treatment, of the resonances at $g_\perp = 2.14$ and $g_\parallel = 1.50$ attributed to [Ru(acac)$_3$] precursor dispersed in the as-prepared xerogel (Figure 1, asterisked line). A very low intensity signal of residual Ru^{3+} centers (less than 1.6% of the total ruthenium)[2] remained; this small amount, with respect to both [Ru(acac)$_3$]−SnO_2 and the species generated further on, caused us to limit the studies on identification. The spectrum, after flowing NO/Ar treatment (RuA_2623 sample), showed well-defined signals certainly attributable to ruthenium centers with d^5 low-spin electronic configuration[8,9] (Figure 1, line b) and was similar to those obtained on Ru−SnO_2 after interaction with CO.[2] According to these previous results,[2] the experimental spectrum was fitted by superimposing three different species that locate Ru^{3+} in the field of oxide anions:[8,9] Ru^{3+}(A) ($g_1 = 2.804$, $g_2 = 2.237$, $g_3 = 1.527$), Ru^{3+}(B) ($g_1 = 2.658$, $g_2 = 2.264$, $g_3 = 1.526$), and Ru^{3+}-(C) ($g_1 = 2.558$, $g_2 = 2.340$, $g_3 = 1.960$) with relative ratios Ru^{3+}(A):Ru^{3+}(B):Ru^{3+}(C) = 2.56:4.67:1 (Figure 1, line b′). After interaction with NO/Ar mixture, the amount of Ru^{3+} increased from 1.6% to about 23% of the total ruthenium.

The amount of paramagnetic Ru^{3+} decreased to about 5.5%, probably because of its reoxidation to Ru^{4+}, when RuA_2623 samples were successively treated under air stream at 298 K

TABLE 2: Mössbauer Parameters for SnO_2 and Ru(Pd,Pt)-Doped SnO_2 Powders at 80.0 K

sample	δ (mm/s)	ΔE_Q (mm/s)	Γ (mm/s)	A (%)
A_1623[a]	0.21(1)	0.55(2)	1.08(4)	91
	0.44(7)	1.32(9)	1.14(9)	9
A_2623[a]	0.22(1)	0.60(1)	1.16(2)	91
	0.42(9)	1.45(8)	1.24(7)	9
B_1623[a]	0.17(1)	0.59(1)	1.03(3)	61
	0.42(5)	0.84(6)	1.41(3)	39
B_2623[a]	0.23(1)	0.57(2)	1.11(3)	83
	0.43(6)	1.37(9)	1.28(9)	17
B_3623[a]	0.14(2)	0.57(2)	1.05(4)	50
	0.39(7)	0.76(7)	1.43(8)	50
RuA_1623	0.24(1)	0.63(2)	1.25(4)	91(4)
	0.43(4)	1.46(7)	0.88(9)	9(4)
RuA_2623	0.21(1)	0.52(2)	0.96(6)	91(9)
	0.41(9)	1.29[b]	1.21[b]	9(5)
RuB_1623	0.22(1)	0.55(1)	1.06(4)	79(5)
	0.38(4)	1.29(5)	1.21(6)	21(5)
RuB_2623	0.21(1)	0.56(2)	1.06(4)	89(4)
	0.40(6)	1.29[b]	1.21[b]	11(4)
RuB_3623	0.22(1)	0.61(2)	1.15(2)	88(2)
	0.50(5)	1.29[b]	1.21[b]	12(3)
PdA_1623	0.18(1)	0.60(2)	1.07(4)	71(5)
	0.49(5)	0.93(6)	1.32(9)	29(5)
PdA_2623	0.20(19)	0.61(1)	1.16(1)	86(2)
	0.41(6)	0.93[b]	1.32[b]	14(3)
PdB_1623	0.19(1)	0.52(3)	0.96(9)	68(4)
	0.36(8)	0.93[b]	1.32[b]	32(9)
PdB_2623	0.19(1)	0.57(2)	1.07(2)	82(4)
	0.42(6)	0.93[b]	1.32[b]	18(7)
PdB_3623	0.19(1)	0.60(2)	1.14(1)	87(4)
	0.55(7)	0.93[b]	1.32[b]	13(5)
PtA_1623	0.22(1)	0.64(1)	1.21(4)	100
PtA_2623	0.22(1)	0.57(1)	1.11(1)	100
PtB_1623	0.22(1)	0.59(1)	1.10(2)	85(1)
	3.02(4)	2.09(8)	1.29(8)	15(2)
PtB_2623	0.22(1)	0.58(1)	1.21(2)	89(1)
	3.05(3)	2.00(5)	1.26(9)	11(2)
PtB_3623	0.21(1)	0.56(1)	1.06(1)	100
PtB_1573	0.23(1)	0.57(2)	1.04(6)	83(6)
	0.38(5)	1.31(8)	1.11(9)	17(5)
PtB_2573	0.22(1)	0.55(2)	1.03(6)	86(6)
	0.38(8)	1.27(9)	1.17(8)	14(7)
PtB_3 573	0.22(1)	0.57(4)	1.21(6)	87(6)
	0.28(3)	1.43(9)	1.05(9)	13(6)

[a] Pure SnO_2 samples (from ref 6). [b] Value constrained to the reported value during the fitting procedure.

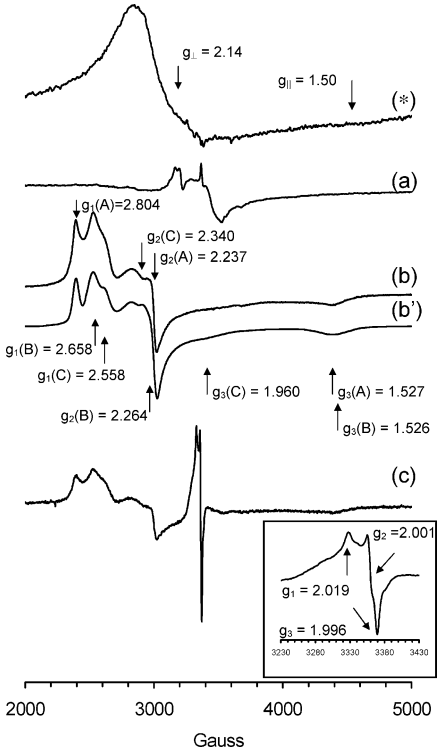

Figure 1. EPR spectra, normalized for the sample amount and the operative conditions, recorded at 113 K, of Ru−SnO_2 treated according to the sequence A: (a) RuA_1623; (b) RuA_2623 (experimental); (b′) RuA_2623 (simulated); (c) RuA_3623. The asterisked line reports the spectrum at 113 K of [Ru(acac)$_3$]−SnO_2 xerogel. In the inset is the spectrum of $Sn_{Sn}-O_2^-$.

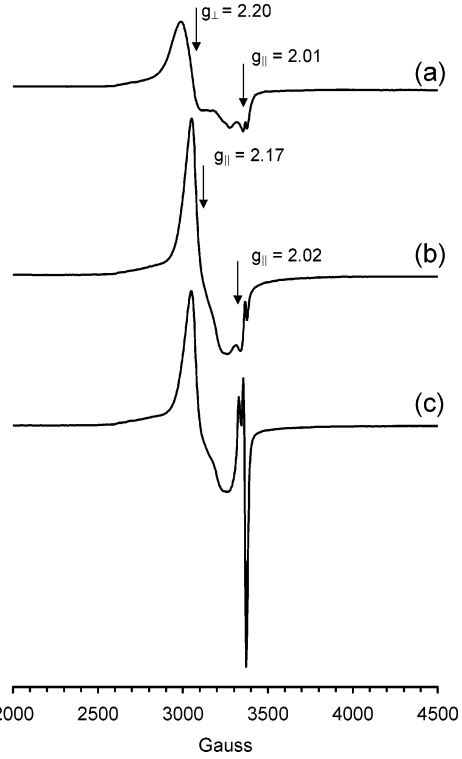

Figure 2. EPR spectra, normalized for the sample amount and the operative conditions, recorded at 113 K on Pd−SnO_2 treated according to the sequence A: (a) PdA_1623; (b) PdA_2623; (c) PdA_3623.

(RuA_3623 samples). The formation of the superoxide paramagnetic species[2] $Sn_{Sn}-O_2^-$, $g_1 = 2.019$, $g_2 = 2.001$, and $g_3 = 1.996$, was observed at the same time (Figure 1, line c and inset); this may be associated with transfer of one electron from Ru^{3+} to O_2, followed by O_2^- chemisorption on Sn_{Sn}. The amount of $Sn_{Sn}-O_2^-$ centers (5 × 10^{15} spin/g) was very low compared with that of Ru^{3+} centers reoxidized to Ru^{4+} (5 × 10^{18} spin/g) and more than 2 orders of magnitude lower than that evaluated after similar air treatment on CO-reduced samples[2] (1 × 10^{18} spin/g).

Pd−SnO_2. Resonance lines with axial symmetry appeared in the EPR spectra (Figure 2 line a) of $PdSnO_2673$ and PdA_1623 samples. On the basis of the **g** tensor values ($g_\perp = 2.20$, $g_\parallel = 2.01$), a low-spin d^7 electronic configuration, due to tetragonally distorted Pd^{3+} centers,[10,11] is proposed. Thus, the oxidation of the xerogel Pd^{2+} centers to Pd^{4+} centers in the matrix of oxide anions involves the formation of Pd^{3+} centers, according to the behavior of PdO_2 which loses lattice oxygen also at room temperature.[12] The amount of paramagnetic Pd^{3+} centers in the PdA_1623 sample was about 15% of the total palladium. After the reaction with flowing NO/Ar at 623 K (PdA_2623 sample), the Pd^{3+} amount increased to 21% of the total palladium and the $g_\perp$ value of 2.20 significantly decreases to 2.17 (Figure 2, line b).

The treatment of PdA_2623 in an air stream at 298 K (PdA_3-623 sample) lowered the amount of Pd^{3+} centers to 15% of total Pd, probably owing to reoxidation. At the same time, a number of paramagnetic $Sn_{Sn}-O_2^-$ centers (3 × 10^{16} spin/g) appeared (Figure 2, line c) and the value was 2 orders of magnitude lower than that of reoxidized Pd^{3+} centers (2 × 10^{18} spin/g).

Pt−SnO_2. Both $PtSnO_2673$ and PtA_1623 samples did not show any EPR signal. This suggested that the precursor Pt^{2+} centers were fully oxidized to Pt^{4+}.

The treatment of PtA_1623 with NO/Ar stream at 623 K (PtA_2-623 sample) also did not produce any resonance. It may be hypothesized that the reduction of Pt^{4+} centers leads to diamagnetic Pt^{2+} or Pt^0 species, in agreement with the behavior of Pt−SnO_2 films under CO interaction.[3] After the treatment with an air stream at 298 K (PtA_3623 sample), the formation of $Sn_{Sn}-O_2^-$ was observed and the number of $Sn_{Sn}-O_2^-$ centers was evaluated to be 1.5 × 10^{17} spin/g. The lack of $Pt^{(4-n)+}$ hindered any comparison with superoxide centers concentration; nevertheless, their formation, due to the electron transfer from the semiconductor to O_2, suggested the reduction of Pt^{4+} centers by NO.

Sequence B. Ru−SnO_2. Several superimposed resonance lines due to different paramagnetic centers appeared in the EPR spectrum of RuB_1623 sample (Figure 3). The lower field group of signals corresponds to Ru^{3+}(A), Ru^{3+}(B), and Ru^{3+}(C) species already observed in RuA_2623, while the higher field signals, typical of low-spin d^5 centers,[8,9] correspond to Ru^{3+}-(D) with less distorted rhombic symmetry, as indicated by **g** tensor values $g_1 = 2.05$, $g_2 = 1.95$, and $g_3 = 1.85$. The total amount of Ru^{3+} centers is not always the same, the value ranging from 20 to 30% of the total ruthenium. The relative intensities of the two groups of signals differed from sample to sample (see Figure 3). It is not unexpected that low-spin Ru^{3+} centers with different surroundings show so large differences in their magnetic tensor values; in fact, the ground state for a low-spin d^5 ion in rhombic symmetry involves the $(xz)^2(xy)^2$-(yz), $(yz)^2(xy)^2(xz)$, and $(xz)^2(xy)(yz)^2$ electronic configurations, whose changes in the relative weight, due to ligand field modifications, induce strong variations of **g** tensor values.[13−16] Similar behavior was reported for ruthenium-exchanged zeolites.[8]

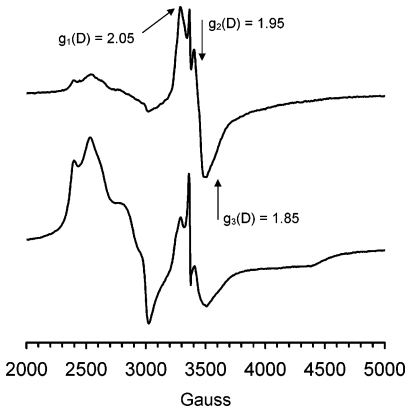

Figure 3. EPR spectra, normalized for the sample amount and the operative conditions, recorded at 113 K on two different RuB_1623 samples.

The subsequent treatment with NO/Ar mixture (RuB_2623 sample) increased the amount of Ru^{3+}(A), Ru^{3+}(B), and Ru^{3+}-(C) species to 30−40% of the total ruthenium, and Ru^{3+}(D) species disappeared or its quantity became very low. The annealing under argon (RuB_3623 sample) did not significantly modify the spectrum of the RuB_2623 sample, except for some slight increase of Ru^{3+}(D) species.

Pd−SnO_2. After being annealed under flowing argon, the sample PdB_1623 showed an increase of Pd^{3+} centers (32% of the total Pd) with respect to $PdSnO_2673$ (15%) and the $g_\perp$ value shifted as previously observed in the case of sequence A (compare PdA_1623 with PdA_2623 samples).

The subsequent treatment with NO/Ar mixture (PdB_2623 sample) slightly decreased the Pd^{3+} centers to 24%, while the final treatment in argon (PdB_3623 sample) increased again the Pd^{3+} centers to 28%. These last two treatments did not induce any other changes of line shape. The Pd^{3+} electronic ground state is probably less sensitive than that of Ru^{3+} to the crystal field modifications. In fact, the low-spin d^7 ground configuration of tetragonal Pd^{3+} centers involves the $(xz,yz)^4(xy)^2(z^2)$ and $(xz,yz)^3(xy)^2(z^2)^2$ electronic configurations, whose changes in the relative weight, due to ligand field modifications, induce less relevant variations in **g** tensor values than the d^5 electronic configurations.[10,11,16] The decrease of Pd^{3+} centers in the PdB_2-623 sample cannot be otherwise explained than hypothesizing the presence of EPR-silent reduced metal species. These are reoxidized after the argon treatment (PdB_3623).

Pt−SnO_2. No signals were observed in EPR spectra, whatever the gas treatment.

The results of EPR analysis showed that NO/Ar treatment on Ru(Pd,Pt)-doped SnO_2 injects electrons to the transition metal centers. Taking into account the $V_o^\bullet$ signals present in the EPR spectra of undoped SnO_2 treated under a NO/Ar mixture[6] and the possible analogy with the CO/Ar interaction of Ru- and Pt-doped SnO_2,[2−5] it may be hypothesized that the reduction is mediated by the oxygen defects through the following main reactions:

$$NO + O_o \Leftrightarrow NO_2(gas) + V_o \quad (5)$$

$$V_o \Leftrightarrow V_o^\bullet + e^- \quad (6)$$

$$M(Ru,Pd,Pt)^{4+} + nV_o^\bullet \Leftrightarrow M(Ru,Pd,Pt)^{(4-n)+} + nV_o^{\bullet\bullet} \quad (7)$$

The electron-transfer reaction 7, occurring as the Fermi energy level of transition metal ions is lower than that of SnO_2 shallow defects ($V_o^\bullet$), should be responsible for the lack of $V_o^\bullet$ resonances in the EPR spectra. This implies that Ru(Pd,Pt)-doped SnO_2, under NO/Ar treatment, lose lattice oxygens, probably those near the transition metal centers, due to the lower strength of the Ru(Pd,Pt)−O_o bond with respect to $Sn_{Sn}-O_o$; also the treatment with pure Ar at 673 K (sequence B) induces the same effects. According to the above statements, one may tentatively explain the difference in magnetic anisotropy among the Ru^{3+} species. The higher magnetic anisotropy of Ru^{3+}(A), Ru^{3+}(B), and Ru^{3+}(C) species could be attributed to a higher number of oxygen vacancies surrounding these three centers with respect to Ru^{3+}(D) ones. These are present in the initial step of sequence B and change into Ru^{3+}(A), Ru^{3+}(B), and Ru^{3+}(C) after contact with NO/Ar atmosphere (MB_2623), presumably due to the increase in the number of surrounding oxygen defects.

It is expected that, beside the main processes (5)−(7), the side reactions 8 and 9 take place:

$$NO + O_O + Sn_{Sn} \Leftrightarrow Sn_{Sn}-NO_2^- + V_o^\bullet \quad (8)$$

$$NO_2 + O_O + Sn_{Sn} \Leftrightarrow Sn_{Sn}-NO_3^- + V_o^\bullet \quad (9)$$

Thus, the low amount of $Sn_{Sn}-O_2^-$ centers, with respect to Ru^{4+} and Pd^{4+} centers, may result from the surface chemisorption of NO_2^- and NO_3^- species, which hinders the interaction of Sn_{Sn} sites with O_2^-.

The conversion of few Ru^{3+}(A), Ru^{3+}(B), and Ru^{3+}(C) centers into Ru^{3+}(D) centers, observed by treating RuB_2623 under Ar atmosphere (RuB_3623), is accounted for by the left-hand shift of reactions 8 and 9 that fills the oxygen vacancies; as well, the reoxidation of Pd^{3+} to Pd^{4+} in PdB_3623 may be due to a back-shift of reactions 8 and 9. It must be emphasized that reactions 8 and 9 both produce $V_o^\bullet$ defects but do not inject electrons to the conduction band.

The sequence B induces a stronger reduction of the material; this was demonstrated by the greater number of Ru^{3+} and Pd^{3+} centers observed after the sequence B. Furthermore, one may think the prolonged annealing in flowing argon induces the formation of oxygen vacancies whose number increases by subsequent interaction with NO, injecting more electrons into the metal centers.

Mössbauer Investigation. The Mössbauer investigation was aimed to recognize the electronic structure of tin in Ru(Pd, Pt)−SnO_2 powders that had undergone sequences A and B at 623 K. The data on transition metal-doped powders are reported in Table 2 and compared with those obtained for undoped SnO_2 under the same treatments.[6]

The spectra of Ru(Pd)−SnO_2 that had undergone sequences A and B at 623 K (Figure 4a) showed the presence of a single absorption around zero velocity; however, any attempt to fit the spectra as either a single line or a paramagnetic doublet failed, due to the presence of a small residual absorption at positive velocity. The spectra were thus fitted, obtaining in every case good χ^2, to two strongly overlapped symmetrical quadrupole split doublets, both with typical parameters of inorganic tin(IV) compounds. It must be stressed that the parameters for the second doublet are affected by large errors, and in some cases they had to be constrained to the reported values, due to the small area and strong overlap with the main doublet. In no case were absorptions due to tin(II) species (for SnO, $\delta = 2.74$ and $\Delta E_Q = 1.93$ mm/s) detected.[17] The first most intense doublet is attributable to SnO_2.[17] The second doublet, much lower in intensity, is due to a tin(IV) species with higher electron density at the nucleus, as proved by the larger δ value. The amount of

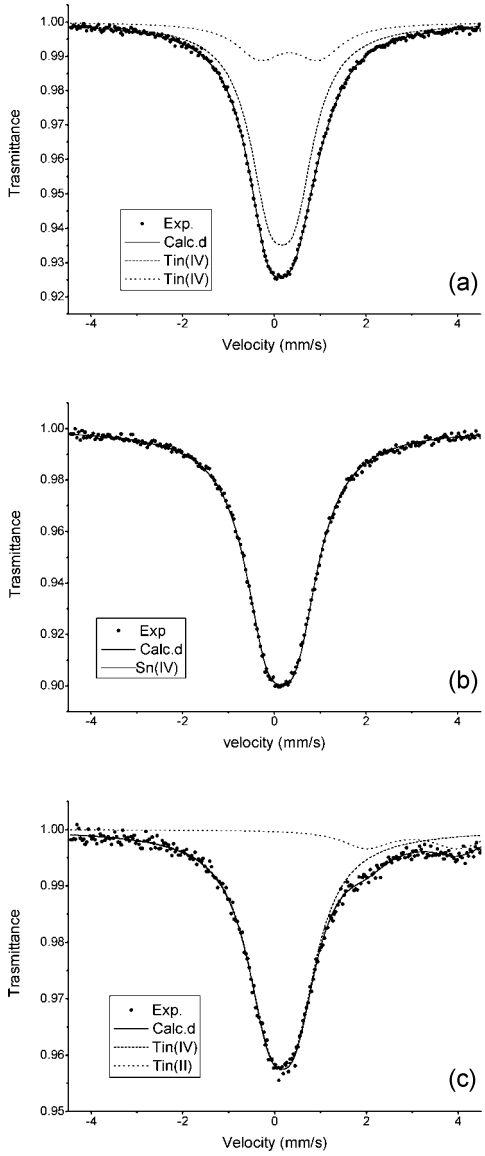

Figure 4. Mössbauer spectra at 80.0 K of (a) RuB_1623, (b) PtA_1623, and (c) PtB_1623.

this latter species is higher in sequence B, in agreement with the larger amount of EPR-active reduced metal centers. For the same sequence B smaller differences between the relative amounts of the two species were observed in samples Ru(Pd)-B_1623, Ru(Pd)B_2623, and Ru(Pd)B_3623 with respect to undoped SnO_2 samples.[6] It seems the doping metal lowers the difference in the charge amount induced on tin(IV) by interaction with gases, in agreement with the reduction mechanism suggested on the basis of EPR results. The electrons trapped into the oxygen vacancies are injected into the conduction band and transferred to transition metal centers (reaction 3), which in turn undergo reduction, without relevant charge effect on the tin centers.

Strong differences were instead observed in charge symmetry as a function of the doping metal, the ΔE_Q average value of 1.29 mm/s for the second Ru−SnO_2 doublet being significantly higher than the value of 0.93 mm/s for the corresponding Pd−SnO_2 doublet. This may suggest that Ru^{3+} centers induce stronger distortion than Pd^{3+} into the symmetry of the electronic distribution around Sn(IV), according to the higher magnetic anisotropy of all the Ru^{3+} centers with respect to Pd^{3+} centers.

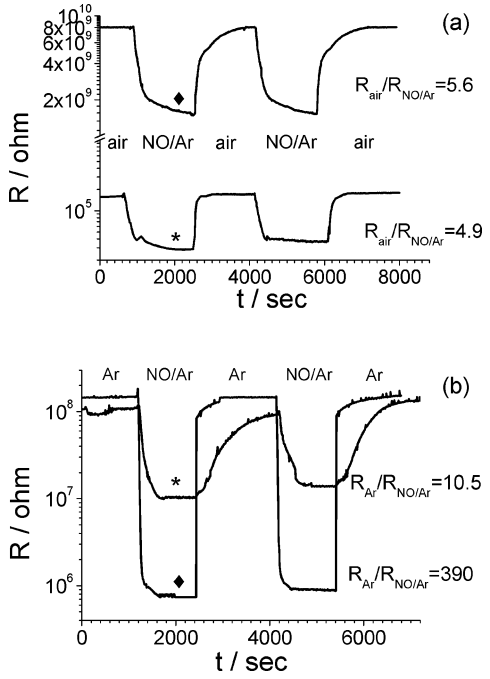

Figure 5. Resistance variations vs time of SnO_2 and Ru-doped SnO_2 films, under a pulse of NO/Argon at 623 K, using (a) sequence A and (b) sequence B. Key: (*) SnO_2; (◆) Ru−SnO_2.

In the case of Pt−SnO_2 that had undergone sequence A, only the first doublet at $\delta = 0.22$ mm/s was evident (Figure 4b); attempts to fit the spectrum with the two tin(IV) absorptions failed.

After sequence B, a second absorption at higher velocity, δ around 3 mm/s and ΔE_Q around 2 mm/s, became evident in samples PtB_1623 and PtB_2623 (Figure 4c). The new doublet, peculiar to Sn(II) species, suggests some of the electrons injected into SnO_2 move from the oxygen vacancies to the tin centers. The final treatment under argon, PtB_3623, probably induces reoxidation of the small amount of Sn(II) to Sn(IV), according to the back-shift of reactions 8 and 9.

Because Pt−SnO_2 showed remarkable electrical sensitivity (see electrical properties) already at a temperature lower than 623 K, the sequence B was performed also at 573 K. The results indicated that at this temperature Pt−SnO_2 behaves as the analogous Ru(Pd)-doped samples, though with higher distortion, ΔE_Q average value of 1.34 mm/s, in the more reduced Sn(IV) species (Table 2). According to this statement, it seems Pt causes for Sn(IV) an electronic distribution of higher distortion than that caused by Ru and Pd. Thus Pt, under reducing conditions, should have greater tendency to segregate, instead of remaining dispersed in the lattice. This clustering effect is expected to increase with the operating temperature and perhaps generates an energy barrier at the phase contact hindering the electron transfer of reaction 7. Under this guess, besides the reduction of Pt^{4+} to $Pt^{(4-n)+}$, one can suppose to take place also the formation of Sn(II) in PtB_1623 and PtB_2623.

Electrical Properties of Ru(Pd,Pt)-Doped SnO_2 Films. Electric resistance measurements of undoped and Ru-doped SnO_2 films that had undergone sequence A and B are reported and compared in Figure 5a,b, respectively. Similar behavior was observed in films doped with the other (Pd, Pt) transition metals. The electrical response of each film is reproducible, even if the electrical conductance is different among films of the same composition. In any case the electrical response is alike among the specimens coming from the same set of composition.

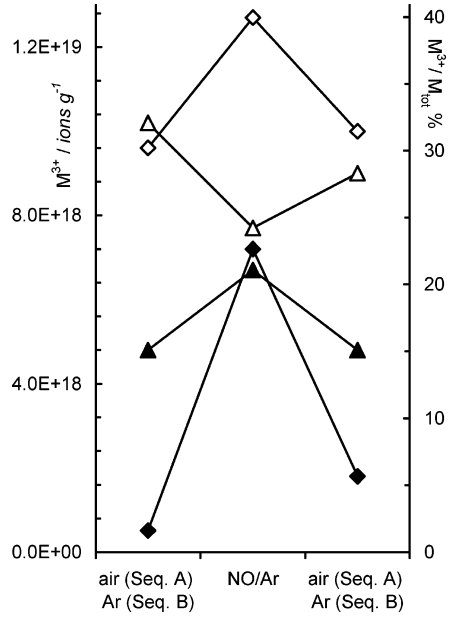

Figure 6. Variation of the number of paramagnetic transition metal centers, expressed as ions g^{-1} (left axis) and % of the total metal (right axis), in sequence A, (▲) Pd−SnO_2 and (◆) Ru−SnO_2, and sequence B, (△) Pd−SnO_2 and (◇) Ru−SnO_2.

Differences in the electrical conductance are generally due to no small difference in film thickness as well as in distance between the measuring electrodes.

The decrease of the electrical resistance, in flowing NO/Ar mixture, suggests electron injection into the oxide by NO and agrees with the reductive effects pointed out by EPR experiments.

The electrical response is significantly enhanced in transition metal-doped samples only when samples underwent sequence B (Figure 5b). The metal effect is very low in sequence A (Figure 5a).

On the basis of the present results, the electron injection into the conduction band due to NO seems to be significantly promoted by a transition metal only if the film was equilibrated under argon (sequence B). This does not agree with the data for EPR measurements (Figure 6): in fact the number of Ru-(Pd)$^{3+}$ centers produced by NO/Ar treatment under sequence A was relevant, despite the low resistance variation. On the contrary, the number of transition metal centers produced by NO/Ar treatment under sequence B was low if compared with the variation of electrical properties and also decreased in the case of Pd. As for sequence B, it may be suggested that NO reduction involves also diamagnetic metal species, injecting further electrons to the conduction band. In sequence A, the relevant amount of reduced transition metal species, with respect to electrical response, may be attributed to reductive effects mediated by reactions 8 and 9 whose electrons ($V_o^{\bullet}$) can be trasferred to metal cationic sites but not injected to the conduction band.

The electrical responses S_B as a function of the operating temperature are reported in Figure 7; their values strongly depend on the nature of the doping metal. Platinum-doped material acts as the best sensitizer also at 523 K, a temperature where the other doping metals show poor effects. It may be suggested that the higher capability of Pt^{4+} centers to trap $V_o^{\bullet}$ defects, with respect to Ru^{4+} and Pd^{4+}, shifts toward the right-hand side the reactions 7, 6, and 5.

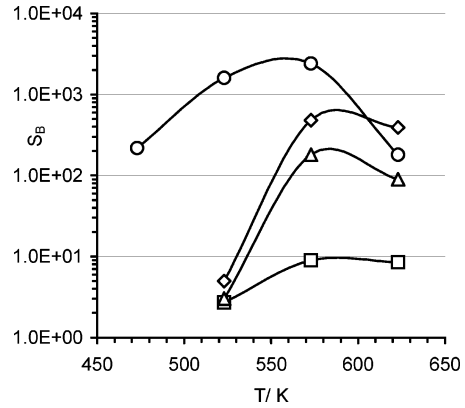

Figure 7. Temperature dependence of S_B (ratio between the film resistance under flowing argon and that under flowing NO/Ar mixture) for the following: (□) undoped SnO_2; (△) Pd−SnO_2; (◇) Ru−SnO_2; (○) Pt−SnO_2 that had undergone sequence B.

The significant decrease in the electrical response of the Pt-doped SnO_2, at 623 K, is probably due to clustering of Pt centers that hinders the electron transfer at the metal−semiconductor contact.

Conclusions

The results reported in this paper demonstrate that the electrical response of Ru(Pd,Pt)-doped SnO_2 to NO is due to the oxygen defect formation (V_o), to their subsequent ionization to $V_o^{\bullet}$, and to injecting electrons into the oxide conduction band.

The localized $V_o^{\bullet}$ electrons are then transferred to M^{4+} centers reducing different amounts of them. This electron transfer allows further interaction of NO with the semiconductor surface promoting both the formation of oxygen defects (reactions 5 and 6) and the electrical response (reaction 2).

The electrical response depends on the dispersion of transition metal centers and on the number of electrons they accept from $V_o^{\bullet}$. This was maximum for Pt^{4+} centers, which have the highest tendency to be reduced[18] compared with Ru^{4+} and Pd^{4+}.

Acknowledgment. This paper is dedicated, on the occasion of his 70th birthday, to Professor Franco Cariati, who back in 1970 first introduced the use of electron paramagnetic resonance investigation to the School of Inorganic Chemistry of the University of Milano.

References and Notes

(1) Yamazoe, N.; Miura, N. *Chemical Sensors Technology*; Yamauchi, S., Ed.; Kodansha Ltd. and Elsevier Science Publishers BV: Tokyo, Amsterdam, 1992; Vol. 4, pp 19−42.

(2) Canevali, C.; Chiodini, N.; Morazzoni, F.; Scotti, R. *J. Mater. Chem.* **2000**, *10*, 773−778.

(3) Morazzoni, F.; Canevali, C.; Chiodini, N.; Mari, C. M.; Ruffo, R.; Scotti, R.; Armelao, L.; Tondello, E.; Depero, L. E.; Bontempi, E. *Chem. Mater.* **2001**, *13*, 4355−4361.

(4) Armelao, L.; Barreca, D.; Bontempi, E.; Morazzoni, F.; Canevali, C.; Depero, L. E.; Mari, C. M.; Ruffo, R.; Scotti, R.; Tondello, E. *Appl. Magn. Reson.* **2002**, *22*, 89−100.

(5) Acciarri, M.; Canevali, C.; Mari, C. M.; Mattoni, M.; Ruffo, R.; Scotti, R.; Morazzoni, F.; Barreca, D.; Armelao, L.; Tondello, E.; Bontempi, E.; Depero, L. E. *Chem. Mater.* **2003**, *15*, 2646−2650.

(6) Canevali, C.; Mari, C. M.; Mattoni, M.; Morazzoni, F.; Scotti, R.; Ruffo, R.; Russo, U.; Nodari, L. *Sens. Actuators, B* **2004**, *100*, 228−235.

(7) Hampden-Smith, M. J.; Wark, T. A.; Rheingold, A.; Huffman, J. C. *Can. J. Chem.* **1991**, *69*, 121−129.

(8) Carl, P. J.; Larsen, S. C. *J. Catal.* **2000**, *196*, 352−361.

(9) Chaudhary, V. A.; Mulla, I. S.; Vijayamohanan, K.; Hegde, S. G.; Srinivas, D. *J. Phys. Chem. B* **2001**, *105*, 2565−2571.

(10) Raizman, A.; Barak, J.; Suss, J. T. *Phys. Rev. B* **1985**, *31*, 5716−5721.

(11) Michalik, J.; Heming, M.; Kevan, L. *J. Phys. Chem.* **1986**, *90*, 2132−2136.

(12) Holleman, A. F.; Wiberg, E. *Inorganic Chemistry*; Academic Press: New York, 1995; p 1521.

(13) Golding, R. M. *Applied Wave Mechanics*; D. Van Nostrand Co. Ltd.: London, 1969; p 278.

(14) Araneo, A.; Mercati, G.; Morazzoni, F.; Napoletano, T. *Inorg. Chem.* **1977**, *16*, 1196.

(15) Mercati, G.; Morazzoni, F. *Gazz. Chim. Ital.* **1979**, *109*, 161.

(16) Drago, R. S. *Physical Methods in Chemistry*; W. B. Saunders Co.: Philadelphia, PA, 1977; pp 492−497.

(17) Geenwood, N. N.; Gibb, T. C. *Mossbauer Spectroscopy*; Chapman & Hall: London, 1971.

(18) Holleman, A. F.; Wiberg, E. *Inorganic Chemistry*; Academic Press: New York, 1995; p 1134.